# THERMAL PERFORMANCE IMPROVEMENT OF ARTIFICIALLY ROUGHENED SOLAR AIR HEATER

**Nabaa M. Bader* – Khudheyer S. Mushatet**

Department of Mechanical, College of Engineering, University Thi-Qar, Iraq

**ARTICLE INFO:**

***Article history*:**
*Received: 07.09.2022*
*Received in revised form: 24.03.2023*
*Accepted: 04.04.2023*

***Keywords:***
*Delta-winglet vortex generator*
*Experimental investigation*
*Heat transfer*
*Ribs*
*Solar air heater*

*DOI: https://doi.org/10.30765/er.2036*

***Abstract:***

*Solar air heaters are useful because they can lessen the need for fossil fuel–powered electricity, thereby lowering emissions and cutting down on energy costs. Experiments were conducted to inspect the thermal performance of a solar air heater with combined ribs and delta-winglet in a single-pass solar air heater. The present goal was boost the thermal performance of a solar air collector. A constant relative roughness height ratio of 0.6 was used to organize eight delta-winglets and seven rectangular ribs on the absorber duct's bottom surface. The attack angles for both winglets and ribs were maintained at 60° and 90°, respectively. The winglet vortex generators were set in a common flow-down configuration with a pitch ratio of 10. This experimental investigation was performed at a mass flow rate of 0.022 kg/s with typical ranges of solar irradiance from 330 W/m2 to 850 W/m$^2$. Results show that the useful energy and thermal efficiency were enhanced by 19.2% and 21.2%, respectively, at maximum solar irradiance compared to a smooth duct. The considered compound ribs and vortex generators affect the temperature of the outlet air, resulting in a considerable improvement in the heat transfer convective rate.*

## 1 Introduction

The combustion of fossil fuels and the production of greenhouse gases are mostly to blame for global warming, air pollution, and other problems, which might lead to catastrophic climatic changes and endanger human health. One of the significant difficulties facing the next generation is how to sustainably provide the human demand for heat, cooling, and power. A workable alternative to traditional power plants is using renewable resources such as sunlight, wave, wind, and tidal energy, among other examples. Solar energy is a significant renewable energy source, and the sun's reflected light and heat. Sunlight may be harnessed using a simple solar air heater, the primary element of solar thermal systems. It warms the moving, cooler air by collecting heat from the radiant sunshine and then transferring that heat to the flowing air. A wide range of applications may be achieved using solar-heated air, such as drying laundry, crops, and lumber, pre-heating ventilation makeup air, and so on. Solar heaters are among the most effective solar thermal systems in terms of efficiency and cost-effectiveness since they are so simple and have an endless supply of air on a human timescale [1-3]. But solar air heating has a lower heat transfer rate than solar water heating.

The air also has a lower thermal conductivity than water, resulting in a lower heat transfer for solar-heater. Consequently, it is necessary to increase the temperature of the solar air heater. The high Reynolds number of the solar air heater causes turbulence to predominate. As we know, Low heat transfer efficiency is caused by the viscous sub-layer in the turbulent boundary layer, where heat conduction dominates. Therefore, it is a valuable method for thinning the boundary layer and improving the blending of the mainstream flow with the flow near the wall.

* Corresponding author:
*E-mail address: nabaa.m@utq.edu.iq*

As a passive method of enhancing heat transmission, vortex generators may be placed on the absorbent plate for the solar collector, where the longitudinal vortex and a transverse vortex are nature's two most common vortices [4]. Generators of longitudinal vortices with delta-winglets (DWVGs) are very efficient. Heat transfer may be boosted since the path of the vortex created is parallel to the main stream wise direction; it may continue for an extended period.

The effect of DWVGs on air heating has been the subject of several investigations. Rajendran et al. [5] tested the efficiency of solar air heaters (SAHs) by placing inclined baffles and winglet on top of the collector surface, besides using flat plates with artificially roughened surfaces. On average, a SAH with inclined baffles was 52.7% efficient, a SAH with winglet was 72.9% efficient, and a SAH with a flat surface is only 30.8% efficient during the experimental day. Khudheyer and Nabaa [6] evaluated the thermal efficiency of a solar air dryer that is integrated with a set of delta-winglet vortex generators (DWVG) put at the bottom surface. In their study, they regarded DWVG eight pairs for relative height (e/H) ratios that ranged from 0.2 to 0.6. According to the findings, the thermal efficiency and useful thermal energy of the rough surfaces solar air dryer at (e/H) value of 0.6 were improved by approximately 6.5% and 9.4%, respectively, compared to a smooth solar air dryer. Kiatpachai et al. [7] discussed the ASP of embedded and welded spiral fin and tube heat exchangers (SFTHXs). While the pressure drop decreased with increasing fin pitch, the friction factor decreased with decreasing fin pitch. A higher heat transfer rate was typically provided by an embedded spiral fin as opposed to a welded spiral fin, because of better connections at the fin base.

The spiral fin with the welds was more effective at reducing pressure than the embedded spiral fin. Khudheyer and Iltifat [8, 9] investigated the interior of a rectangular duct with an array of winglet vortex generators and various geometrical configurations, including rectangular, semi-circle, triangular and parabolic. It is generated on the bottom heated surface with the ability to change the attack angle from 0 to 60°. They demonstrated that the proposed vortex generator configuration of common flow-up improves heat transfer and thermal performance by 240 % and 170 %, respectively. Further, a significant rise in heat transfer improvement and thermal performance is observed when the locations and the angle of attack between the vortex generators increase. Ribs, which have the potential to create transverse vortices, assist in the mixing of the fluid that is close to the wall. Meanwhile, impoundment and reconnection of fluid toward the ribs can considerably improve heat transmission. After investigating the heat transfer rate in a flat plate solar air heater (SAH), Nidhul et al. [10] found that a passive technique offered the best chance of success. Using fins, turbulators, or ribs on the surface indicated a passive method. Research into the exergetic performance of these rib configurations shows that including additional ribs and/or rib-gaps improves exergetic efficiency compared to V-rib SAH by 12% and 31.6%, respectively. Bezbaruah et al. [11] analyzed the impact of a solar air heater with modified conical vortex generators in a staggered arrangement for varying relative pitch ratios (from 2.67 to 15) and varying relative height ratios (0.17 to 0.34). Using a staggered configuration of modified conical vortex generators improved thermal performance by 257%.

The best thermo-hydraulic performance parameter was 2.04. Thianpong et al. [12] examined the thermal behavior of isosceles triangular ribs attached to two opposed duct walls at AR = 10. They concluded that the optimal thermal performance of stagger ribs might be around e/H = 0.1 and P/H = 1.0. Varun et al. [13] and Hans et al. [14] conducted extensive literature surveys from over a hundred references on several ribs turbulators. Hajabdollahi [15] suggested a unique setup wherein a liquid solar thermal collector was combined with a fin. It was determined that an efficiency of 0.6359 was achievable for the best possible heat transfer rate. The mass flow rate of air must also be greater than the mass flow rate of water. The ratio of air to water mass flow rate rises for heat transfer rates between 0 and 60 kW and falls for rates above 60 kW. According to Hakan et al. [16], the heat transfer rate raised as the obstruction's aspect ratio rises, which was affected by the step height. The researchers discovered that an increase in the obstruction aspect ratio results in a lower pressure drop. According to Khudheyer and Sarah [17,18], discrete ribs that are correctly structured provided better heat transfer on the duct wall than continuous ribs.

They discovered that among the cases examined, continuous ribs follow the case of intermittent-continuous-intermittent ribs and have the lowest performance factor. In contrast, intermittent ribs had bigger friction factor values. Further, experimental work was tested out by Khudheyer and Nabaa [19], employing parallel ribs at various angles of attack (30°, 45°, and 60°) in a solar air heater under solar simulation system settings at 0.022kg/s MFR). Compared to a rib with a 90°, hot outlet air temperature increased by 8 %, 14 %, and 17 %, respectively. In the thermal performance evaluation, the 60° rib had the best Nusselt number and covered the largest surface area compared to the other cases. It has also been shown by Mushatet [20] that

increasing the contraction ratio improves both strength and area of the recirculation zone behind the step. Because of a step height that has gone up. A reduction in the reattachment zone area following ribs and their length was seen with an increased contraction ratio. As well as affecting the Nusselt number and the change in turbulent kinetic energy, the contraction ratio and Reynolds number also have an effect. As previously established, both transverse and longitudinal vortices significantly affect heat transfer. The DWVGs and ribs may be attached to the absorber plate of a solar air heater beneficially. Promvonge et al. [21] investigated the thermal-hydraulic performance of a solar receiver heat exchanger (SRH) equipped with a unique longitudinal-vortex generator, a trapezoidal louvered winglet, and a wavy groove inserted into the absorber.

The best thermal performance was achieved at PR of 1.5, with BR of 0.4 providing almost 2.6. Kumar and Apurba [22] intended to improve the thermal performance of solar air heater using a liquid crystal thermography (LCT) approach, an improved type solar air heater consists of winglet-type rib roughened surface. These experimental findings were enhanced by 17% to 46 % under the provided conditions as compared to the smooth channel. Zhao et al. [23] evaluated the convective heat transfer enhancement and friction loss behaviors for turbulent airflow. The heat transmission performance of the DWVG paired with 60° V-shaped continuous ribs is determined to be the greatest, with a 39.4 % over the case of solely WVG. Sunil et al. [24] studied the flow and thermal features of SAH integrated with the winglet vortex generator. The findings reveal that the winglet vortex generator with c/a= 0 and ß= 30° offers the optimum TEF range of (1.72 - 2.20), while the most significant Nu and f values are found at ß = 60° and c/a=1. As far as the authors know, previous research on roughened solar air heaters has examined a small subset of their potential performance characteristics. Combined delta-winglet vortex generators and ribs have received only a limited amount of research. As part of the current investigation, an experimental study was conducted to evaluate the thermal efficiency and outlet air temperature of the solar air heater.

The goal of this research is to determine whether the addition of artificial roughness can increase the thermal performance and heat transfer rate of SAH. On top of the absorber plate (that has a thickness of 0.07 mm) are the delta-winglets vortex generators (DWVG) in their deployed positions. It formed a stream wise common flow-down configuration with a pitch ratio (P/e) of 10. The transverse ribs (TR) are put between the winglet pairs with an (e/H) of 0.6 for both the ribs and the winglets. SAH is heated by using a solar simulation system, and the solar irradiance varies hourly from 330 W/m2 to 850 W/m2. The solar air heater has four cases: a smooth plate, a plate roughened with eight pairs of DWVG, a plate roughened with eight TR, and a plate with combined roughness (CSAH) for a fixed MFR of 0.022 kg/s.

## 2 Experimentation

### *2.1 Experimental Setup*

An experimental setup with the essential structure of the solar simulator test system for a solar air heater has been created using delta-winglet vortex generators paired with rib turbulators laid on an absorbent plate. The photograph and schematic diagram of the experimental setup is displayed in Figure 1 and Figure 2, respectively.

*Figure 1. Experimental photograph view of the test rig.*

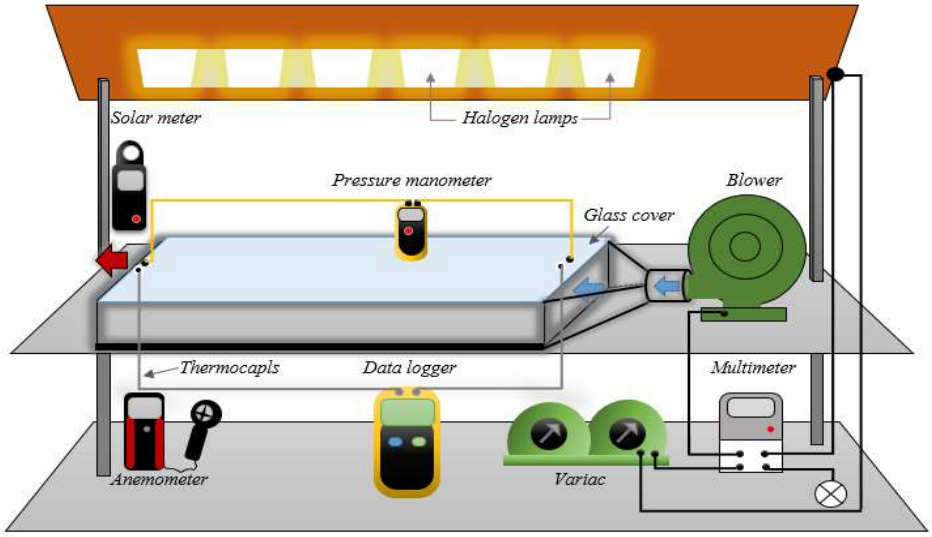


*Figure 2. Schematic diagram of the test rig.*

It is not reasonable to say, "The solar spectrum is equal to the spectrum of the halogen lamp." The solar spectrum has all colours and is called white light, and it has a wide and equal wavelength, while the lamp has a shorter wavelength and more concentration. The incandescent lamp is a temperature radiator. The light is generated by heat and therefore the lamp has the full light spectrum. It comes close to the warm- white light of the sun in the evening. Compared to sunlight (Figure 3), the colour spectrum of the incandescent lamp (Figure 4) has a much lower blue component, and the light distribution rises sharply and continuously towards the red and infrared components. These properties make the incandescent lamp the ideal light source for warm-white color temperatures. As for the transmittance and absorption glass of the duct, as it depends on the gained natural radiation. [25]

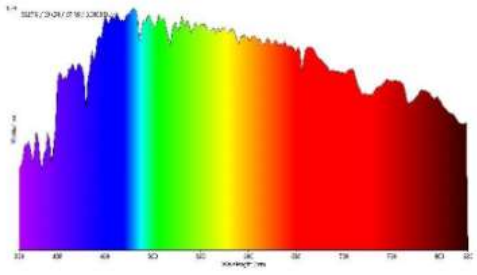

*Figure 3. The sunlight spectrum is quite balanced.*

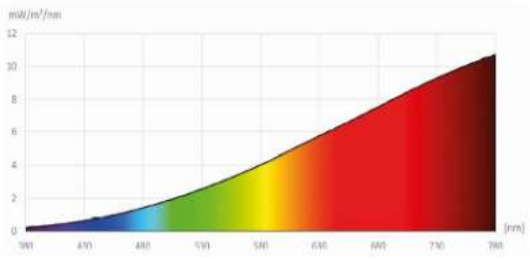

*Figure 4. The spectrum of a lamp. [25].*

Further, the collector is a device that aims to convert the thermal energy contained in the sun's rays or solar radiation into a form that is more usable and stored. Therefore, the results of the collector's thermal performance when using halogen lamps are near or similar to the results of the collector using sunlight, being the same intensity of measured solar radiation.

The halogen lamps, glass cover, and solar air duct with dimensions of 1250 mm length, 360 mm width, and 50 mm height, respectively, together with an absorbent plate of roughness, are the primary components of the solar simulation system, including the solar heater as depicts in Figure 5. Six halogen lamps, each rated at 500 watts, were used to provide the absorber plate with the necessary heat. Throughout the experiment, a tilt of 31.054° was chosen for the solar air heater location. A gap of 150 mm was determined to provide the most accurate measurement of solar irradiance intensity when placed between the halogen lamps and the glass cover. It is a material that allows, under normal temperature conditions, sunlight to pass through. Glass is characterized by a clear, homogeneous transparency, through which all light rays pass from ultraviolet to

infrared. Glass also has the ability to reflect and refract light. The refractive index of glass ranges between (1.467-2.179). One of the characteristics of glass is that it is resistant to thermal shock. Which means it can withstand sudden temperature changes well. It is also able to withstand extreme heat and cold, to different degrees. Also, absorbing heat better than metal, glass can reflect, bend, transmit and absorb light with great precision. [26]

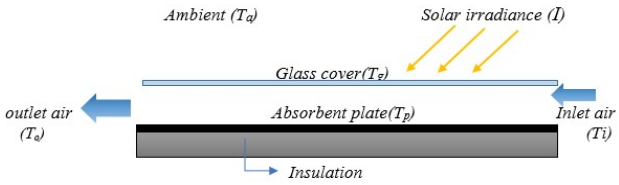


*Figure 5. Single-pass solar air heater.*

The primary aim of the current research is to investigate and analyze the effect of transverse ribs being paired with delta-winglet vortex generators. Before being secured, the delta-winglet (DWVG) was mounted on an absorbent plate at 150 mm a distance from the plate's edge. The DWVG has dimensions of 50 mm length and 30 mm height. The pitch ratio (p/e) of 10, as well as a gap of 10 mm between the delta-winglet tip (δ). It formed a common pair that moves downward at an angle of attack (ß) of 60°. As for the ribs (TR), it has dimensions of 350 mm, 20 mm, and 30 mm. TR is positioned in the middle of the winglet pairs, transversely at an angle of attack (α) set at 90º with the main flow. Also, the pitch ratio of 10 is between one rib and another. These are likewise coloured with a black thermal dye, as shown in Figure 6. Where the above dimensions were determined on several different researches and after conducting experiments on several different measurements in order to obtain the best thermal performance of the solar collector.

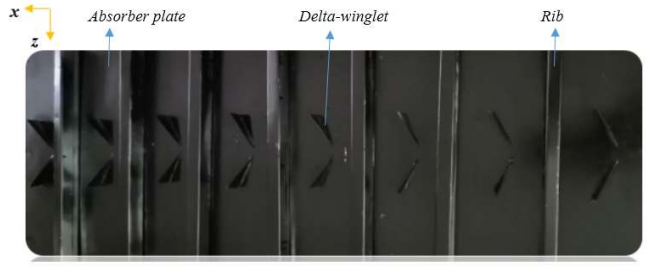


*(a) photograph view of CSAH.*

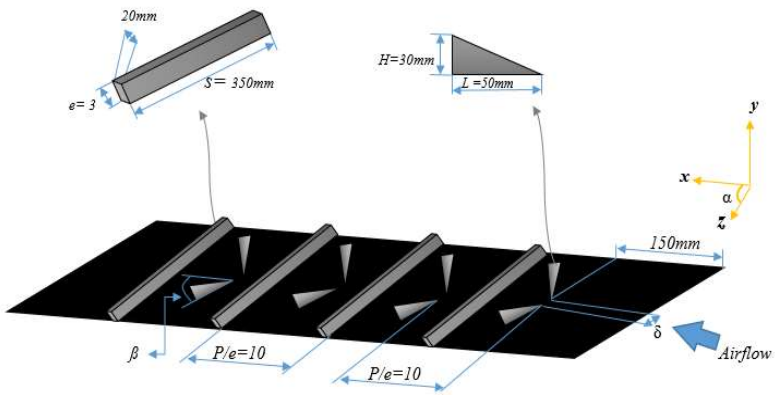


*(b) Schematic view of CSAH.*

*Figure 6. (a) and (b) Arrangement of CSAH on absorber plate in solar air heater.*

*2.2 Experimental procedure*

The variables to be monitored were selected and reported hourly, from 8 AM to 4 PM. Among these variables are mass flow rate, solar irradiance, the temperature of ambient, inlet and outlet air temperature, and absorbent plate temperature at several pre-selected locations. The blower (model 3", 2800-3000 RPM) is used to push air into the SAH. A consistent MFR was obtained using a speed controller connected to the blower to regulate the flow velocity. The halogen lamps were turned on, and their radiation intensity was adjusted using variac to match this irradiance with the actual solar radiation. The SAH performance is examined beneath four absorbent plate cases (i.e. smooth plate only, absorber plate with TR, absorbent plate with DWVG, and absorbent plate with CSAH.

The performance of the SAH with a fixed air MFR (0.022 kg/s) was examined to determine the impact of employing winglets and ribs. Ten (K-type) thermocouple sensors were arranged among four matrices to monitor the temperature on the bottom surface of the absorber plates. In addition, two thermocouple sensors are fitted at the duct's entry and outlet for reporting temperatures. The temperature values are displayed by through connected these sensors to an SD card data logger (Model: BTM-4208SD) with accuracy (±0.4%+1°C), range (-50 to + 999.9° C). Accurately ± (3%+0.5) digital anemometer is used to measure airflow rates. In contrast, the intensity of solar radiation is measured by solar power meter type (A SWAR) (model AS-M582), with the accuracy of ± (4% rdg + 8 dgts).

*2.3 Experimental data reduction*

The characteristics of turbulent airflows, such as the Reynolds number and the Nusselt number, are deduced from the airflow velocity, the average wall temperature, and the inlet and outlet airflow temperature along the rectangular duct. These variables were measured in the experiments with and without the presence of turbulators for several cases. In this experimental effort, the working fluid was monitored while it flowed turbulently through a rectangular duct exposed to varying solar irradiation levels. In this section, the essential equations that are required to compute the variables are evaluated:
In order to calculate the mass airflow rate, one must:

$$m^{\cdot} = \rho_a \, U_m \, A_c \tag{1}$$

Calculating the SAH's thermal efficiency requires the following formula: [23]

$$\eta = \frac{Q_u}{I \; A_{\mathrm{sur}}} \tag{2}$$

To get the absorber plate's surface area, use the equations:

$$A_{sur} = L \, W \tag{3}$$

The useful thermal energy is gained as: [30]

$$Q_{\mathrm{u}} = \dot{m} \, C_{\mathrm{p}} \, (T_{\mathrm{o}} - T_{\mathrm{i}}) \tag{4}$$

An expression for the mean heat transfer coefficient may be found:

$$h = \frac{Q_u}{A_{sur} \, (T_o - T_i)} \tag{5}$$

In situations in which the temperature of the absorber plate is achieved by:

$$T_p = \frac{1}{n} \, (\Sigma T_{pi} \tag{6}$$

Mean bulk temperature is achieved through the following, which include:

$$T_b = \frac{(T_o + T_i)}{2} \tag{7}$$

The following is a rough estimation of the Nusselt number: [27]

$$N_u = \frac{h\, D_h}{k} \tag{8}$$

The hydraulic diameter is achieved by:

$$D_h = \frac{4A_c}{p} \tag{9}$$

$$p = 2(W + H) \tag{10}$$

$$A_c = W\, H \tag{11}$$

The Darcy equation can define the friction factor as: [30]

$$f = \frac{2\, \Delta P\ D_h}{L\, \rho\, U_{avrg}^2} \tag{12}$$

The thermal-hydrodynamic performance (overall performance) factor which compromises the heat transfer enhancement and pressure drop, is calculated as: [28]

$$¥ = \frac{(Nu/Nu_o)}{\sqrt[3]{(f\ /f_o)}} \tag{13}$$

where, $f_o$ and $Nu_o$ are the friction factor and Nusselt number of the smooth SAH, respectively.

*2.4 The uncertainty*

The three-times over test has been done to verify the correctness of the findings of the experimental work under identical conditions to estimate outlet air temperature and thermal efficiency for CSAH at MFR = 0.022 kg/s and $I$ = 850 W/m$^2$. The difference between the three tests was less than 0.56 % regarding thermal efficiency. Table 1 shows the measurement uncertainties and the resulting data. Calculated the uncertainty from the following equations:

The mean, $\overline{X}_{mean}$ [17]

$$\overline{X}_{mean} = \overline{X}_{average} = \frac{\sum_1^n X_i}{n} \tag{14}$$

$X_i$ denotes each value of measurement, and n is the total number of x measurements. Standard deviation is represented by σ:

$$\sigma = \sqrt{\frac{\sum_1^n (X_i - \overline{X})^2}{n-1}} \tag{15}$$

The standard deviation of the mean is a metric for determining how far something deviates from the mean $\sigma_m$:

$$\sigma_m = \frac{\sigma}{\sqrt{n}} \tag{16}$$

The true measured value of (x) is given:

$$x = \bar{x} \pm \sigma_m = \bar{x} \pm \frac{\sigma}{\sqrt{n}} \tag{17}$$

*Table 1. Uncertainties of measured and resulting data.*

| Parameter | Uncertainty |
|---|---|
| Outlet air temperature | ±2.29°C |
| Air MFR | ±0.15 kg/s |
| Solar radiation | ±3 W/m$^2$ |
| Efficiency | ±0.56% |

## 3 Results and discussion

The heat transfer characteristics of the solar air heater with combined roughened absorbent plates have been evaluated. Just several clear days in January provided the perfect conditions for the tests. During daylight, the intensity of solar irradiation and ambiance temperature is recorded at one-hour intervals and then applied to the solar simulation system. This research concentrated on outlet air temperature trends, useful thermal energy, and thermal efficiency and is shown in the forms:

### *3.1 Outlet air temperature and solar radiation intensity.*

The SAH was exposed to solar irradiation half an hour before the measurements were recorded. Fig. 7 represents the variance in outlet air temperature over time for TR, DWVG, and CSAH, as well as a smooth SAH at MFR of 0.022 kg/s. The hourly solar radiation increases from 8:00 AM to 1:00 PM, decreasing after that. The outlet air temperature is initially 37°C using CSAH because of the heat gained by the fluid (air) within the heater. It increases until 1:00 PM owing to an increase in solar intensity, after which it falls as solar irradiance declines.

The temperatures of the outlet dropped sharply at 4:00 AM because of a decline in the thermosiphon phenomena. In this case, the highest temperature of outlet air was 58.5°C at 1:00 PM, and solar intensity was likewise at its peak. At the time of maximum solar irradiation, the smooth plate experienced the most extraordinary outlet air temperature of 40°C. The temperature improved in case 1 by 13% when using eight pairs of DWVG, and it enhanced in case 2, eight of TR by approximately 20%. While the temperature improved in case 3 when using CSAH by around 25% compared to a smooth SAH. Since DWVG creates vast longitudinal vortices and, according to the variations in the thickness of the free-stream layer downstream of the DWVG pair, the thickness of the free-stream layer decreases as the stream advances. It is worth noting that the reduction in the thickness of the boundary layer helps improve heat transmission, which should be kept in mind. As a result, the vortex pair that DWVGs cause transports the fluid to both sides, reducing the thickness of the free-stream layer but causing the layer to accumulate along the midway. That's to say, the winglet vortex generates a pair of counteracting pushing forces, and the strength of these forces reduces as the flow moves forward. For 90° ribs, longitudinal vortices hit the transverse ribs. Inducing transverse vortices is possible and creates more intricate secondary flows and an even more turbulent airflow field, which leads to the intensified blending of hot and cold air. Besides transferring heat from the fluid's surface to its core, transverse vortices can transport heat in the opposite direction. Transverse vortices improve heat transmission. Longitudinal vortices, as opposed to transverse ones, spiral the flow around their axes. As a result, longitudinal vortices may persist downstream for several vortex generator lengths. Vortices, both transverse and longitudinal, promote

heat transfer by destabilizing flow. Where the heat transfer area in SAH with ribs and vortex generators increased by 20% compared to SAH with smooth plate.

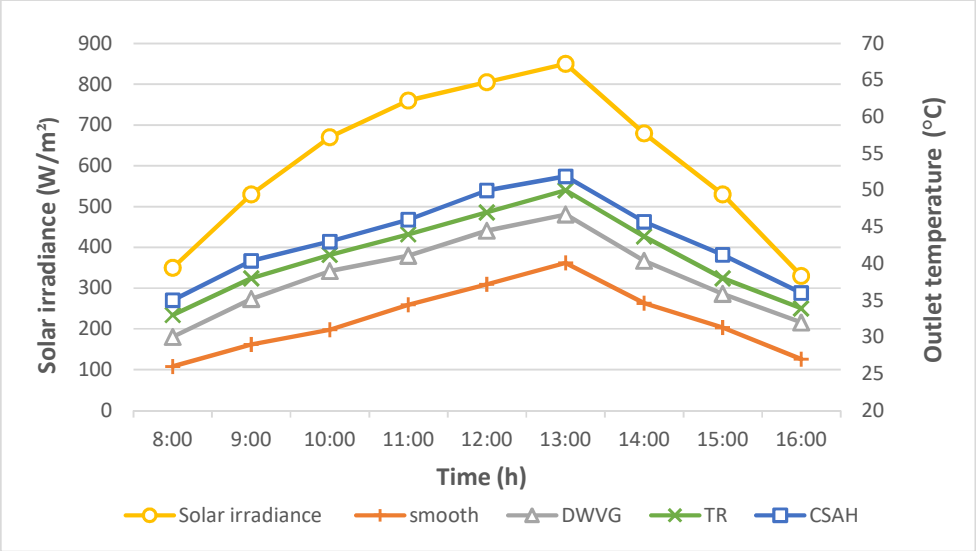


*Figure 7. Variation in outlet air temperatures and hourly solar irradiance for the investigated cases.*

*3.2 The useful hourly energy and temperature difference.*

Figure 8 intended to be evaluated the useful thermal energy ($Q_u$) of solar air heaters having roughness variations under the influence of varying hourly solar irradiance. It may be noticed that the interpretation was semi-linear, increasing until noon when the maximum value was attained and then decreased. The CSAH has large values of useful energy by 19.2 % compared with a smooth SAH for a constant MFR of 0.022 kg/s.

The explanation is that the maxima values of the hot output air temperature have been established, and the temperature differential continues to widen. As a direct result, the amount of $Q_u$ is growing. Varying hourly solar irradiance and the type and the arrangement of roughness surface affect the temperature differential ($T_o$ - $T_i$), as shown in Figure 9. Initially got ($T_o$ - $T_i$) was 2.8°C for CSAH.

The estimations start to increase dramatically when the maximum value is attained by 9.9° C at 1 PM because of an increase in solar irradiation. After that, it decreased with the decrease in solar irradiation at 4 PM The rising in the outlet air temperature is the reason for the increase in the ($T_o$ - $T_i$), whose increment is approximately linear.

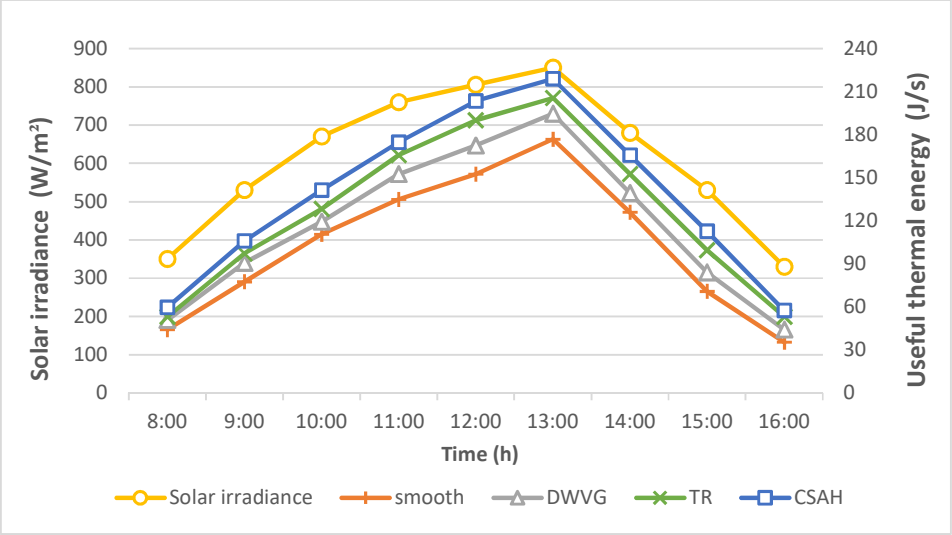


*Figure 8. Variation in useful energy and hourly solar irradiance for the investigated cases.*

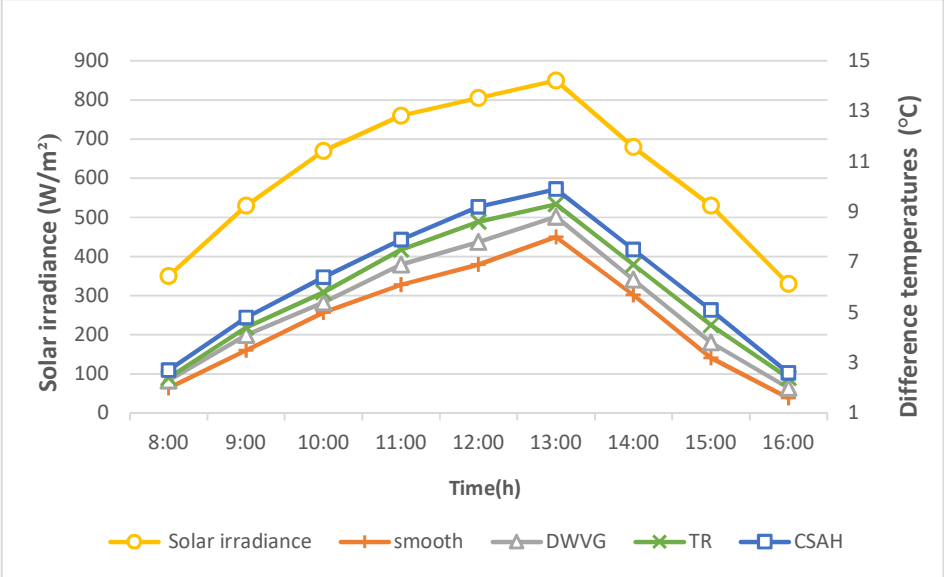


*Figure 9. Variation in difference temperatures and hourly solar irradiance for the investigated cases.*

### *3.3 The hourly Nusselt Number and thermal efficiency.*

The variation in the Nusselt number (Nu) that occurs when solar radiation acts against a variety of rough surfaces is depicted in Figure 10, which may be found here. According to the findings, the Nu increases with increasing solar irradiance, whereas the MFR remains fixed at 0.022 kg/s throughout the study. The Nu with the CSAH is about 2.1 times that of the smooth duct during midday.

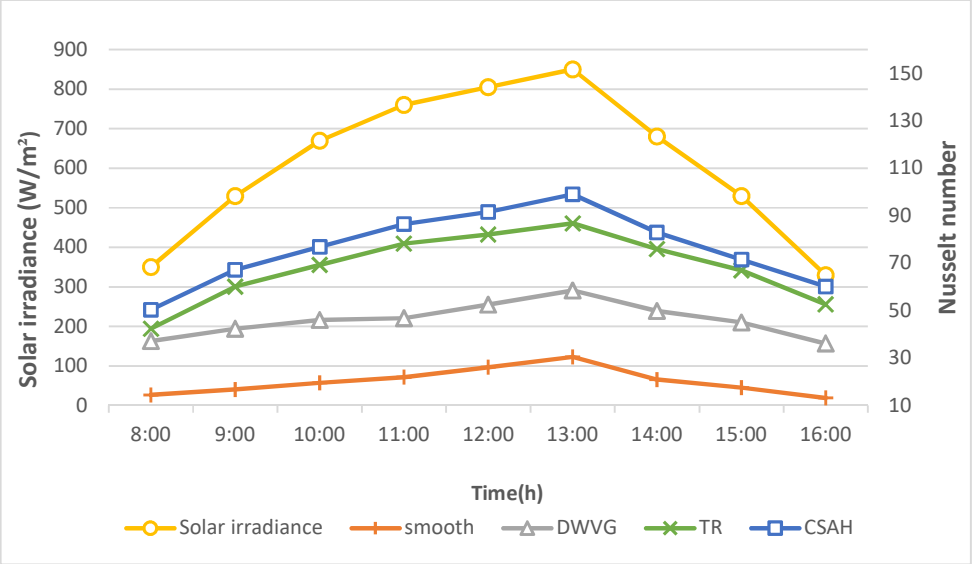


*Figure 10. Variation in Nusselt number and hourly solar irradiance for the investigated cases.*

The effect of DWVG, TR, and CSAH, as well as a smooth SAH on thermal efficiency at MFR of 0.022 kg/s, is illustrated in Fig.11. The collected data reveals a comparable trend in thermal efficiency variation with different hourly solar irradiance in January. Initially, thermal efficiency increases with the rise of solar irradiance to attain a maximum at 1 PM (semi-linear variation or it increases gradually, straight, and not wobbling), and then, it starts to fall. It is noticed that the thermal efficiency corresponding to the greater ratios of DWVG is better at 11.5% compared to a smooth SAH. This effect can be ascribed to the fact that the DWVG inhibits the primary flow and hence generates the secondary flow, which is responsible for this result and then spreads along the DWVGs. Introducing DWVGs causes longitudinal vortices, which disrupt the boundary layer's formation. The boundary layer's leading edge is thinner, which improves thermal efficiency. In reality, disrupting and mixing the flow will alter the original flow and temperature field, and the flow separation point and recirculation zone would be delayed for the streamlined arrangement.

The increased area ratio of the winglet vortex generators causes more significant boundary layer disruption. It improves airflow mixing, where these longitudinal vortexes allow hot and cold fluids to interact for extended periods. As well the flow pattern inside the duct also indicates this turbulence strength. Thus, the heat transmission rate improves. Either TR and CSAH are improved by 16.5% and 21.2%, respectively, compared to a smooth surface. This impact may be attributed to the roughness's ability to restrict the main flow, which creates the secondary flow accountable for this consequence and then spreads throughout the duct. The rib is the location where the separation takes place, and it is this spreading free shear layer that may be found downstream from the separation point.

The reattachment point is the birthplace of a reverse flow boundary layer, which continues to increase in thickness in the upstream region. After passing through the reattachment point, the boundary layer redevelops itself. When the reverse flow and recirculation zone regions meet, the wall shear stress is at zero, but it begins to rise again after reaching that state. In the neighborhood of a reattachment point, the greatest heat transfer occurs. The longitudinal swirls mixed with transverse vortices allow hot and cold fluids to interact for extended periods. The flow pattern inside the duct also shows this turbulence strength. Thus, the heat transfer rate increase. [29]

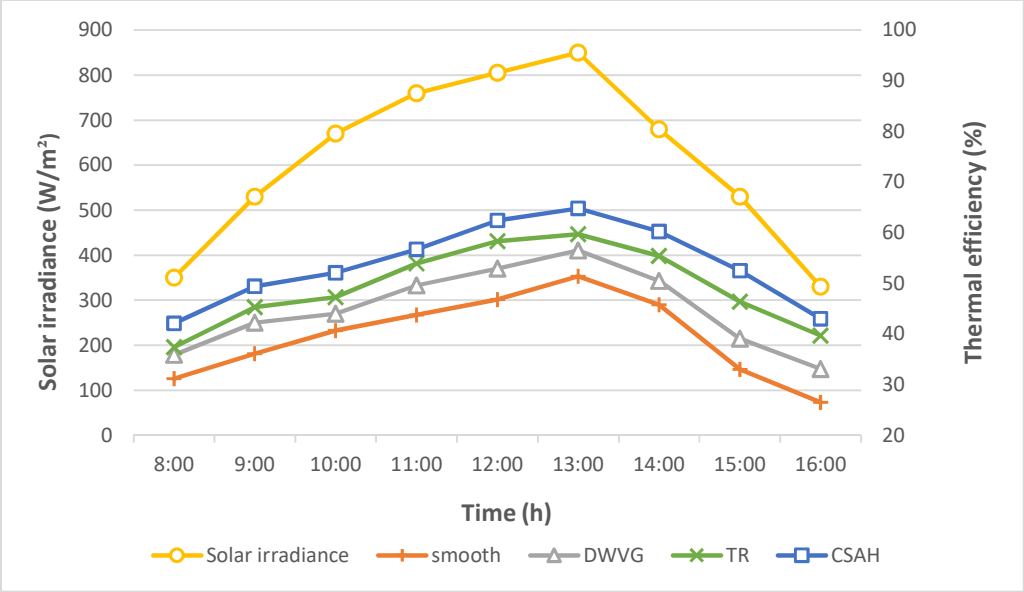


*Figure 11. Variation in thermal efficiency and hourly solar irradiance for the investigated cases.*

*3.4 Comparison between the published and present results.*

In this study, the results are validated in terms of the Nusselt number for the smooth SAH, the present experimental data, the numerical data from Sunil et al. [24], the experimental data from Anil et al. [30], and the Dittus–Boelter equation ($Nu = 0.023\ Re^{0.8}\ Pr^{0.4}$) [31] of Nusselt number for smooth rectangular duct are compared, as shown in Figure 12. the Prandtl number was calculated from equation ($Pr = \mu\ C_p / k$) [32] at $5000 \leq Re \leq 14000$.

The average absolute deviation of the current study is 7.2%. Nusselt number deviates 8.3% between the recent findings for a smooth SAH and those of Sunil et al. [24]. This validation shows that the current study forecasts are relatively precise.

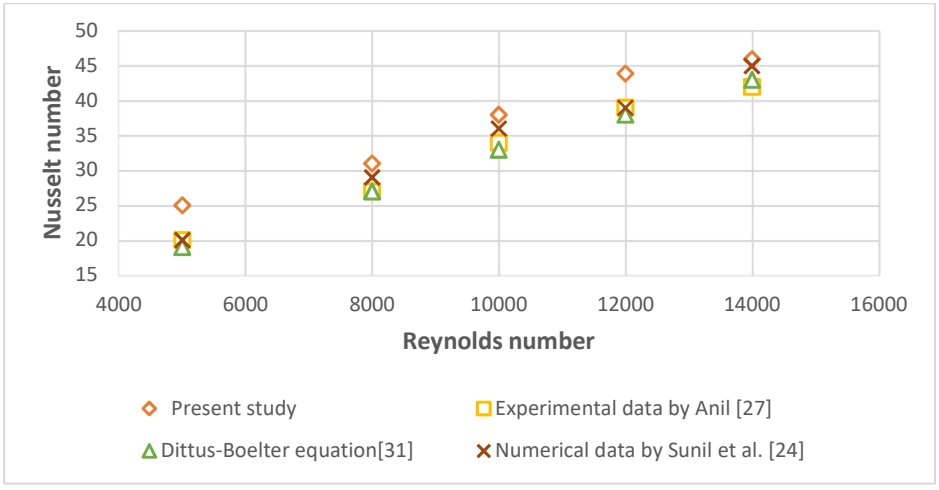


*Figure 12. Comparison of Nusselt number for a smooth solar air heater.*

*3.5 Pressure drop, friction factor and overall performance*

In this study, all the pressure losses, denoted by the symbol (ΔP), comprise losses caused by friction factor ($f$) and losses caused by the drag force produced by artificial roughness. It has been discovered that the case

of CSAH displays the greatest values for friction, whilst the case of DWVG delivers the least value for the friction factor. In addition, the fluctuation of the friction factor concerning the Reynolds number of ducts that have been outfitted with a variety of artificial roughness arrangements. It has been observed that raising the Reynolds number results in a reduction in the friction factor. The comparison is showed by a connection between the Reynolds number and the friction factor at Reynold number from 5000 to 14000 see in Figure 13.

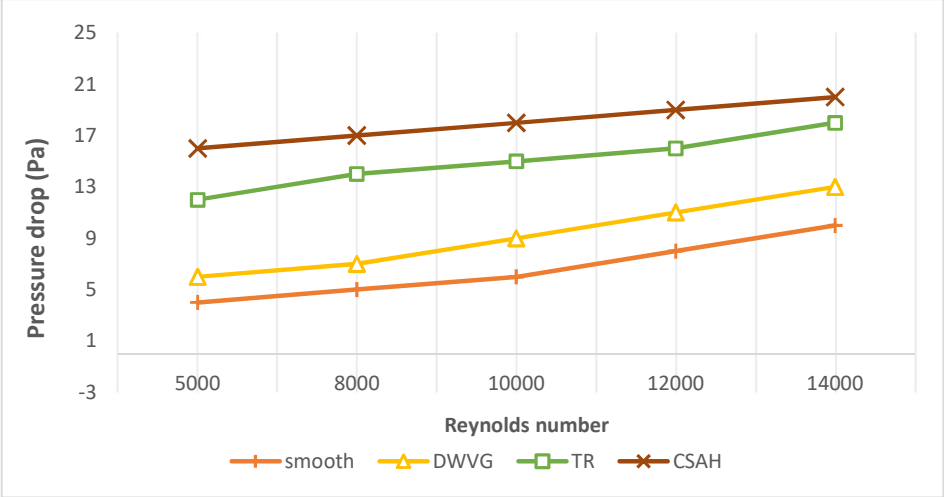


*(a)*

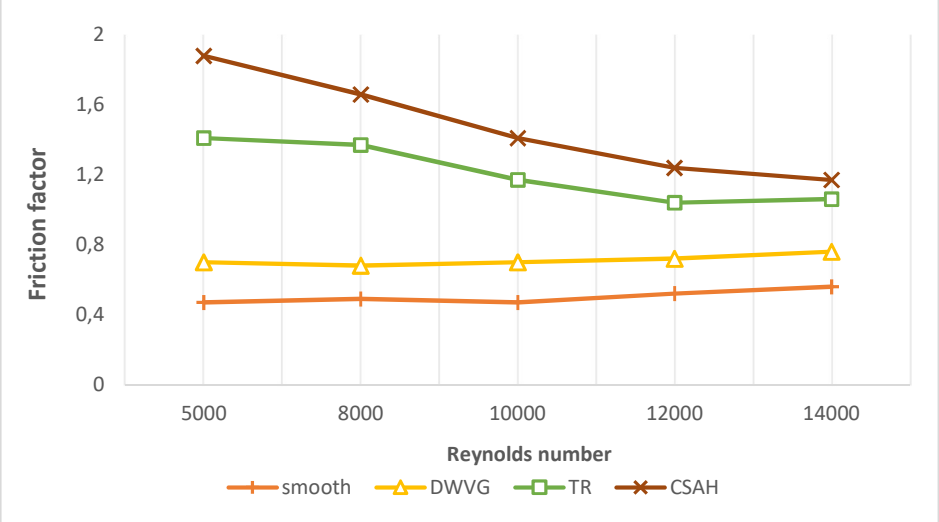


*(b)*

*Figure 13. The variation of (a) pressure drop and (b) friction factor with Reynolds number for roughened and smooth SAH.*

In the presence of artificial roughness, the fluctuation of the overall performance factor as a parameter of MFR is depicted in Figure 14. It has been observed that the overall performance improves at TR and even more so than CSAH in every instance of MFR values. However, this results from increased friction. The MFR has a deleterious correlation with performance because a higher MFR results in a lower total or hydraulic performance because of the reduction in friction. This relationship is inverse.

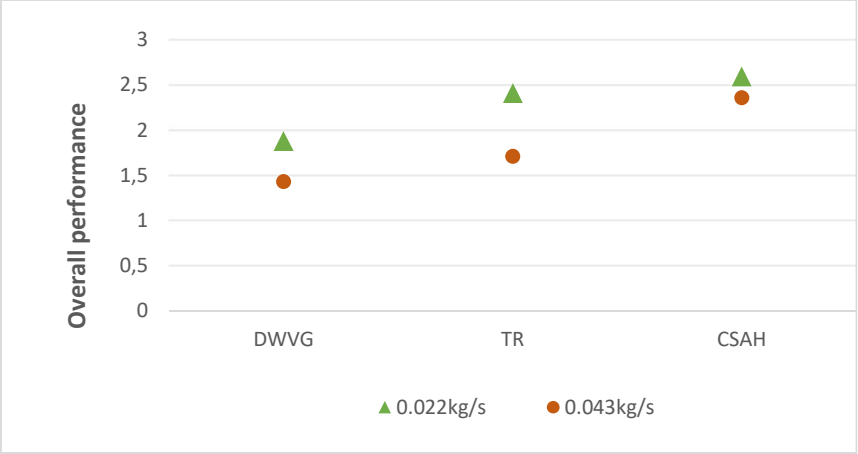


*Figure 14. The variation in overall performance with MFR for artificial roughness.*

## 4 Conclusion

The impact of transverse vortices generated by the TR combined with the longitudinal vortices generated by DWVG above the absorbent plate of single-pass SAH has been examined experimentally at a constant velocity of inlet air of 0.022 kg/s. The solar irradiance intensity was prepared through the solar simulation system, similar to the weather, ranging hourly from 330 to 850 W/m$^2$. According to the outcomes of the tests, this case of CSAH in solar collector increased the heat transfer region and turbulence intensity of the stream of air and thus enhanced the thermal performance. The following is a brief description of the main conclusions:

1. The thermal efficiency of the SAH with combination ribs and winglets (CSAH) was enhanced by 21.2% compared to a smooth SAH.
2. Nusselt number for CASH increased by 2.35 times compared to a smooth SAH.
3. The temperature differences between the exit airflow and inlet increased by using CSAH was equal to 9.9°C at 850 W/m$^2$ maximum solar irradiance.
4. The outlet air temperatures for DWVG, TR, and CSAH improved by about 14%, 19.8%, and 23%, respectively, at 1 PM as contrasted to a smooth SAH.
5. The authors are on the path of developing the solar air heater with a double-pass design and opposite-pass with different turbulators generators.

## References

[1] Raitila J, and Tsupari E, "Feasibility of solar-enhanced drying of woody biomass," *Bioenerg Res*, vol. 13, pp. 210-221, 2019.

[2] Chemkhi S, Zagrouba F, and Bellagi A, "Drying of agricultural crops by solar energy," *Desalination*, vol. 168, pp. 101-109, 2004.

[3] Jamali B, Rasekh M, Jamadi F, Gandomkar R, and Makiabadi F, "Using PSO-GA algorithm for training artificial neural network to forecast solar space heating system parameters," *Appl Therm Eng,* vol. 147, pp. 647-660, 2019.

[4] Stritih U, Charvat P, Klimes L, Osterman E, Ostry M, and Butala V, "PCM thermal energy storage in solar heating of ventilation air-experimental and numerical investigations," *Sustain Cities Soc*, vol. 37, pp. 104-115, 2018.

[5] Rajendran, V., Singaraj, K., and Rajarathinam, J. "Environmental, economic, and performance assessment of solar air heater with inclined and winglet baffle," *Environmental Science and Pollution Research*, pp. 1-16, 2022.

[6] Mushatet, K. S., and Bader, N. M., "Experimental investigation for the performance of the solar air dryer with vortex generator," *In Defect and Diffusion Forum*, vol. 419, pp. 57-67, 2022.

[7] Kiatpachai, P., Kaewkamrop, T., Mesgarpour, M., Ahn, H. S., Dalkılıç, A. S., Mahian, O., and Wongwises, S., "Air-side performance of embedded and welded spiral fin and tube heat exchangers," *Case Studies in Thermal Engineering*, vol. 30, pp. 101721, 2022.

[8] Khudheyer S. Mushatet, and Iltifat lazim edan, "Effect of winglet vortex generators orientation on heat transfer enhancement," *International Journal of Mechanical & Mechatronics Engineering IJMME-IJENS*, vol. 18, pp. 8-24, 2018.
[9] Khudheyer S. Mushatet, and Iltifat lazim edan, "Effect of winglet vortex generators configuration on thermal performance of a heated rectangular channel," *University of Thi-Qar Journal for Engineering Sciences*, vol. 10, pp. 64- 83. 2019.
[10] Nidhul, K., Yadav, A. K., Anish, S., and Kumar, S. "Critical review of ribbed solar air heater and performance evaluation of various V-rib configuration," *Renewable and Sustainable Energy Reviews*, vol. 142, pp. 110871., 2021.
[11] Bezbaruah, P. J., Das, R. S., and Sarkar, B. K., "Experimental and numerical analysis of solar air heater accoutered with modified conical vortex generators in a staggered fashion," *Renewable Energy*, vol. 180, pp. 109-131, 2021.
[12] Thianpong C, Chompookham T, Skullong S, and Promvonge P. "Thermal characterization of turbulent flow in a channel with isosceles triangular ribs," *Int Commun Heat Mass Transfer*, vol. 36, pp. 712–717, 2009.
[13] Varun, Saini RP, and Singal SK, "A review on roughness geometry used in solar air heaters," *Solar Energy*, vol. 81, pp. 1340–1350, 2007.
[14] Hans VS, Saini RP, and Saini JS, "Performance of artificially roughened solar air heaters – a review," *Renew Sustain Energy Rev*, vol. 13, pp. 1854–1869, 2009.
[15] Hajabdollahi, H., "Thermoeconomic assessment of integrated solar flat plat collector with cross flow heat exchanger as solar air heater using numerical analysis," *Renewable Energy*, vol. 168, pp. 491-504, 2021.
[16] Hakan F. Oztop, Khudheyer S. Mushatet, and İlker Yılmaz, "Analysis of turbulent flow and heat transfer over a double forward-facing step with obstacles," *International Communications in Heat and Mass Transfer*, vol. 39, pp. 1395–1403, 2012.
[17] K. Mushatet, and S. Nashee, "Experimental and computational investigation for 3-D duct flow with modified arrangement ribs turbulators," *Thermal Science*, vol. 25, pp. 1653-1663, 2021.
[18] S.R. Nashee, and K.S. Mushatet, "3D numerical and experimental analysis for turbulent flow and heat transfer in a duct integrated with ribs turbulators," *TEST engineering and management,* vol. 83, pp. 21810-21821, 2020.
[19] Khudheyer S. Mushatet, and Nabaa M. Bader, "Thermal performance assessment for the solar air collector integrated with ribs turbulators under Nassiriya city climate," *Journal of Mechanical Engineering Research and Developments, JERDFO*, vol. 45, pp. 166-174, 2022.
[20] Khudheyer S. Mushatet, "Simulation of turbulent flow and heat transfer over a backward-facing step with ribs turbulators," *Thermal Science*, vol. 15, pp. 245-255, 2011.
[21] Promvonge, P., Promthaisong, P., and Skullong, S., "Experimental and numerical thermal performance in solar receiver heat exchanger with trapezoidal louvered winglet and wavy groove," *Solar Energy*, vol. 236, pp. 153-174., 2022.
[22] Kumar, Amit, and Apurba Layek, "Evaluation of the performance analysis of an improved solar air heater with Winglet shaped ribs," *Experimental Heat Transfer,* vol. 35, pp. 239-257, 2022.
[23] Zhiqi Zhao, Lei Luo, Dandan Qiu, Zhongqi Wang, and Bengt Sunden, "On the solar air heater thermal enhancement and flow topology using differently shaped ribs combined with delta-winglet vortex generators," *Energy*, vol. 224, pp. 119944, 2021.
[24] Sunil Chamoli, Ruixin Lu, Dehao Xu, and Peng Yu, "Thermal performance improvement of a solar air heater fitted with winglet vortex generators," *Solar Energy*, vol. 159, pp. 966-983, 2018.
[25] Schlegel, G. O., Burkholder, F. W., Klein, S. A., Beckman, W. A., Wood, B. D., and Muhs, J. D., "Analysis of a full spectrum hybrid lighting system," *Solar Energy*, vol. 76, pp. 359-368, 2004.
[26] Roy, A., Ghosh, A., Mallick, T. K., and Tahir, A. A., "Smart glazing thermal comfort improvement through near-infrared shielding paraffin incorporated SnO2-Al2O3 composite," *Construction and Building Materials*, vol. 331, pp. 127319, 2022.
[27] M.M.K. Bhuiya, A.K. Azad, M.S.U. Chowdhury, and M. Saha, "Heat transfer augmentation in a circular tube with perforated double counter twisted tape inserts," *Int. Commun. Heat Mass Transfer,* vol. 74, pp. 18–26, 2016.

[28] A. M. Bagabir, J. A. Khamaj, and A. S. Hassan, "Turbulent Periodic Flow and Heat Transfer in a Square Channel with Different Ribs," *International journal of heat and fluid flow*, vol. 5, pp. 67–80, 2013.

[29] Kabeel, A. E., Attia, M. E. H., Zayed, M. E., Abdelgaied, M., Abdullah, A. S., and El-Maghlany, W. M., "Performance enhancement of a v-corrugated basin hemispherical solar distiller combined with reversed solar collector: An experimental approach," *Renewable Energy*, vol. 190, pp. 330-337, 2022.

[30] Kumar, A., Saini, R. P., and Saini, J. S., "Experimental investigation on heat transfer and fluid flow characteristics of air flow in a rectangular duct with Multi v-shaped rib with gap roughness on the heated plate," *Solar Energy*, vol. 86, pp. 1733-1749, 2012.

[31] Ba, T. L., Gróf, G., Odhiambo, V. O., Wongwises, S., and Szilágyi, I. M., "A CFD study on heat transfer performance of SiO2-TiO2 nanofluids under turbulent flow," *Nanomaterial*s, vol. 12, pp. 299, 2022.

[32] Ramesh, G. K., Kumara, B. C., Gireesha, B. J., and Reddy Gorla, R. S., "MHD stagnation point flow of nanofluid towards a stretching surface with variable thickness and thermal radiation," *Journal of Nanofluids*, vol. 4, pp. 247-253, 2015.